Frequency lock-in phenomenon for self-sustained roll oscillations of rectangular wings undergoing a forced periodic pitching motion

L. Tregidgo, Z. Wang, and I. Gursul
University of Bath, Department of Mechanical Engineering, Bath BA2 7AY, United Kingdom

(Received 30 April 2012; accepted 2 October 2012; published online 28 November 2012)

The free-to-roll behaviour of rigid and membrane rectangular wings with an aspect ratio of two was studied in wind tunnel experiments conducted at a chord Reynolds number of $Re_c = 46\,000$. Self-excited roll oscillations resulting from the fluid-structure interaction were studied in forced sinusoidal pitching motion in order to simulate gust encounters of small air vehicles. For the dynamic pitching cases, the frequency and phase of the self-excited roll oscillations can become synchronized (or locked-in) with the fundamental pitching frequency and its subharmonics. This is believed to be the first documented example of synchronization for this type of fluid-structure interaction. Depending on the amplitude and frequency of excitation (pitching motion), there are regions of decreased roll oscillations, which may be important for the gust response of small vehicles. © *2012 American Institute of Physics*. [http://dx.doi.org/10.1063/1.4767468]

I. INTRODUCTION

Limit-cycle roll oscillation of slender delta wings, known as wing rock, is a well-known fluid-structure interaction.[1,2] It is not limited to *slender* delta wings only, but also observed for *non-slender* delta wings.[3,4] For delta wings, this fluid-structure interaction is driven by the interaction of the leading-edge vortices with the wing. Recent experiments showed that these limit-cycle roll oscillations are also possible for other wing shapes, including rectangular and elliptical wings,[5,6] and for aspect ratios up to 4.0. The onset of these oscillations may occur at increased angles of attack, but still below the stall angle. For all wings, interaction of the tip vortices with the wing drives the limit-cycle roll oscillations.

These observations have important implications for small aircraft flying at low Reynolds numbers.[7,8] Due to their operation in the atmospheric boundary layer, small aircraft will be extremely susceptible to gust loads. This is particularly important in an urban environment where local, architecturally induced gust loads may be present. Small aircraft may be subject to vertical or horizontal gusts. In particular, vertical gusts may induce self-sustained roll oscillations as the effective angle of attack increases during the gust. Based on the gust amplitude and speed of the aircraft, the effective angle of attack may vary by up to 10 degrees.[9] The free-to-roll dynamics is a first step towards better understanding of the gust response of small aircraft.

In this paper, we intend to study the nature of the self-sustained roll oscillations in a vertical gust. For this purpose, we choose the simplest form of the gust simulations: periodic pitching motion. Experimentally, pitch/plunge motions as models of a vertical gust are often preferred due to their simplicity. Figure 1 shows the main variables. The wing is subject to a forced periodic motion in the form of $\alpha_{pitch} = \alpha_0 + A\sin(2\pi f_{pitch}t)$, where f_{pitch} is the pitching frequency. Depending on the wing mean angle of attack α_0, when $f_{pitch} = 0$, the wing may exhibit self-sustained roll oscillations with a natural frequency f_0. The response of the wing roll angle to sinusoidal pitch excitation will be studied as the pitching frequency f_{pitch} and amplitude A are varied. It is expected that self-sustained roll oscillations may be locked into the excitation (pitching) frequency for some frequencies and amplitudes. This is known as synchronization.[10] In the field of fluid dynamics, this phenomenon

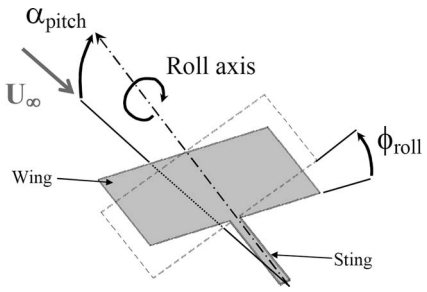

FIG. 1. Schematic of the free-to-roll experimental setup with definition of pitch and roll axes.

was observed for vortex shedding from oscillating cylinders,[11,12] periodically forced wakes,[13] wake of plunging airfoils,[14] jet impingement on an oscillating leading-edge,[15] and oscillating airfoils in transonic buffeting flows.[16] It can be said that, in each case, there is a self-sustained oscillator with a natural frequency. When the excitation frequency is close to the natural frequency, the self-sustained oscillator begins to oscillate at the excitation frequency. This is called frequency lock-in, or synchronization.

The present study aims to understand how the roll oscillations may be locked-in with the gust (pitching) frequency. This is achieved by performing experiments at a low Reynolds number with two free-to-roll wings in forced periodic pitching motion for various frequencies and amplitudes. To the best of our knowledge, such experiments were not conducted previously, with the exception of the work by Khan *et al.*[17] on slender delta wings. In their paper, the authors considered the cases when $f_{\text{pitch}} = 1/2f_0, f_0, 2f_0$ only. In our study, f_{pitch} was varied continuously in a wide range, and the regions of synchronization were identified.

II. EXPERIMENTAL SETUP

Tests were conducted for free-to-roll wings at a chord Reynolds number $\text{Re}_c = 46\,000$ in the closed-loop, open-section wind tunnel at the University of Bath. The tunnel has a working section diameter of 760 mm. A schematic of the experimental setup is shown in Figure 2(a).

A. Wing design and construction

Both rigid and flexible (membrane) wings were tested. Both wings were of a rectangular, perimeter-reinforced design and constructed using the same aluminium frame with overall chord-length of 70 mm and an aspect-ratio of two (Figure 2(b)). The frame had a thickness of 2 mm, chosen to ensure structural rigidity whilst maintaining a thin-aerofoil profile. Different 'skins' were bonded onto the frame to produce the final test specimens: for the membrane wing, the skin used was latex of thickness $h = 0.2$ mm, density $\rho_m = 1$ g/cm^3 and Young's Modulus $E = 2.2$ MPa; whilst for the rigid wing the skin consisted of steel shim with a thickness $h = 0.15$ mm. The characteristics of the membrane wing, combined with the chosen freestream velocity $U_\infty = 10$ m/s, gave a value of 5.90 for the aeroelastic parameter defined by Smith and Shyy,[18]

$$\Pi = \left(\frac{2Eh}{\rho U_\infty^2 c}\right)^{\frac{1}{3}}. \tag{1}$$

The values of the aeroelastic parameter and Reynolds number are in the ranges used in previous investigations,[19,20] $\Pi = 3.5$ to 7.5, $\text{Re}_c = 50\,000$ to $150\,000$.

B. Free-to-roll device

Freedom of rotation about the roll axis was achieved through low-friction ball bearings, mounted in a housing together with a 500 count-per-revolution optical encoder, which provided a non-contact

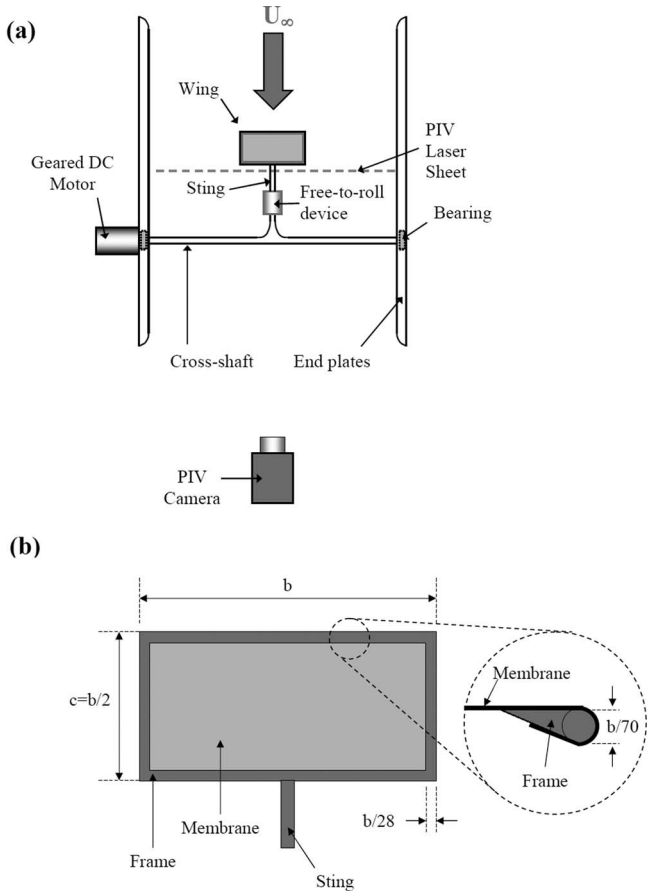

FIG. 2. Experimental setup for free-to-roll tests showing (a) plan-view schematic of system setup, (b) details of wing geometry and construction.

means of measuring the wing roll angle, ϕ_{roll}. A resolution of 0.18° was achieved in the final roll data output. The sampling frequency was 100 Hz. Measurements were conducted for a duration of 60 s, repeated three times and averaged. Mean and RMS quantities were seen to converge to within 2.5% of a steady state value in all cases.

C. Pitch control

Pitch control was provided by a geared DC motor, connected to the wing and free-to-roll device by a shaft spanning between the working section endplates. The pitching axis was located at a distance of 110 mm behind the wing trailing-edge. Precision control of the motor position allowed the pitch angle of the wing to be adjusted remotely to within ±0.25°. For the dynamic pitch cases an analogue drive signal based on a sinusoidal waveform was fed to the motor's controller.

D. Particle image velocimetry (PIV) measurements

A 2D PIV system was used to take measurements of the flow field in a cross-flow plane behind the wing trailing edge at a distance of $\Delta x/c = 0.3$ (see Figure 2(a)). This plane was selected in order to capture the location and strength of the two tip vortices generated by the wing, which from the work of previous studies are believed to be the driving force behind self-excited roll oscillations.[2,6] Measurements were phase-locked to the pitching motion. The PIV capture frequency varied from 4.4 Hz to 11.2 Hz. The PIV data presented in this paper are instantaneous images of the flow-field, selected so as to be representative of the wing behaviour for a given set of the pitching

parameters. Illumination of the desired measurement plane was achieved using a ND:YAG laser with a maximum output of 50 mJ per pulse. Images were captured with a 2 mega-pixel CCD camera located downstream of the wing and accurate timing between laser and camera was achieved using a synchroniser. A multi-jet, compressed-air atomiser was used to seed the flow with olive oil and resulted in a mean droplet diameter of 1 μm. The images were analysed using Insight 3G software running an FFT cross-correlation algorithm and a Gaussian peak engine. Recursive interrogation was used with an initial grid size of 56 pixels and a final grid size of 28 pixels, resulting in a vector spatial resolution of 1.33 mm. The estimated velocity measurement uncertainty was 2% of the freestream value.

E. Force measurements

To provide a baseline of the wing performance, measurements were taken of the chord-normal force coefficient C_N for both rigid and membrane wings at stationary incidence angles in the range $0^\circ \leq \alpha_{\text{pitch}} \leq 30^\circ$. In these cases, the free-to-roll device was disabled and the wing was fixed at $\phi_{\text{roll}} = 0^\circ$. Force data were recorded using a single component load cell with a maximum load capacity 0.3 N. The load cell formed an integral part of the sting such that force was measured in a chord-normal direction. Signals from the load cell were fed via an amplifier to an Analogue-Digital Converter (ADC) sampling at 1 kHz. Each stationary wing data point was averaged over a period of 60 s. Normal force was calculated from the voltage signal by way of linear calibration curves that were generated at the start and end of every run. The total measurement uncertainty in the normal force coefficient was calculated as 5.5%.

III. RESULTS

A. Fixed-incidence cases

The chord-normal force coefficient results for rigid and membrane wings, ($0^\circ \leq \alpha_{\text{pitch}} \leq 30^\circ$), are shown in Figure 3. Both wings generated small positive force values at $\alpha_{\text{pitch}} = 0^\circ$ due to the non-zero camber profile. In the case of the rigid wing, this was produced by the rigid frame at the leading-edge and trailing-edge (see Figure 2(b)). For the membrane wing, the deformation of the membrane provided the additional lift at zero angle of attack. At all angles of attack tested, the membrane wing generated larger values of C_N owing to the increased camber created as the latex skin deformed under aerodynamic load. The membrane wing also stalled at a higher angle ($\alpha_{\text{stall}} = 23^\circ$ compared to $\alpha_{\text{stall}} = 20^\circ$ for the rigid wing) and generated a maximum force coefficient $C_{N,max}$ that was 31% greater. These results are consistent with previous research.[19,21,22]

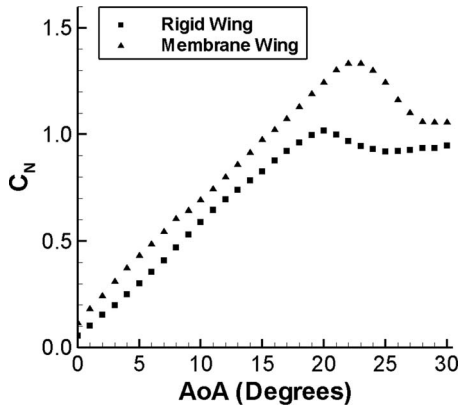

FIG. 3. Variation in normal force coefficient (C_N) over the incidence range $0^\circ \leq \alpha_{\text{pitch}} \leq 30^\circ$ for rigid and membrane wings with rectangular planform. $Re_c = 46\,000$.

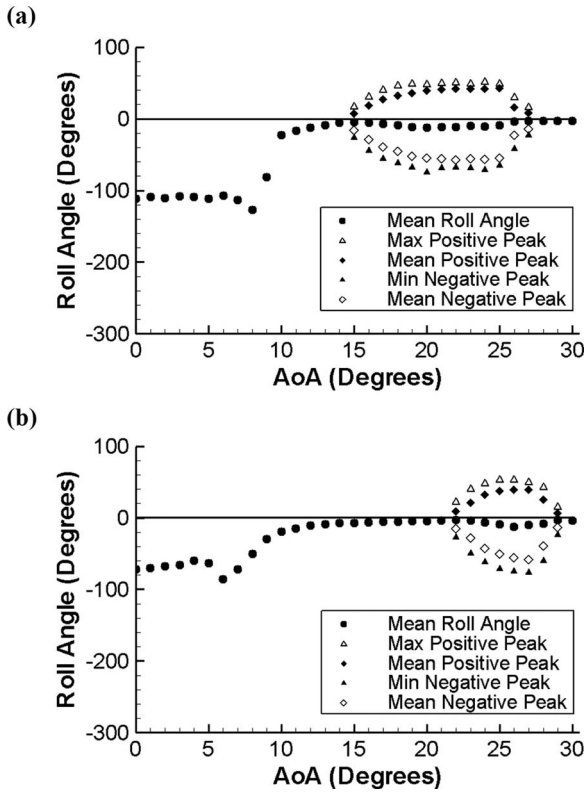

FIG. 4. Mean and peak roll angles plotted against angle of attack for (a) rigid wing, and (b) membrane wing. $Re_c = 46\,000$.

With the free-to-roll device now enabled, measurements of the rolling behaviour for both wings were recorded over the same incidence range (see Figure 4). In general, the features of both plots can be split into four regions:

1. Steady, large non-zero roll angles

At incidence angles up to $\alpha_{pitch} \approx 9^\circ$, both wings found an equilibrium position at large, steady, non-zero roll angles. The largest time-averaged value recorded was $\phi_{mean} = 127^\circ$ for the rigid wing at $\alpha_{pitch} = 8^\circ$. Gresham *et al.*[6] reported similar behaviour in low aspect-ratio rectangular wings, and attributed it to the asymmetric formation of the leading-edge separation bubble. It has been shown that the leading-edge profile is important and the roll asymmetry vanishes for a sharp leading-edge.[6]

2. Steady, near-zero roll angles

Beyond the first region of steady, large non-zero equilibrium angles there was a range of incidence angles for which the wings stabilised near $\phi_{mean} \approx 0^\circ$. Again, the equilibrium angles were steady with no signs of limit-cycle oscillations developing. For the rigid wing this regime spanned $10^\circ \leq \alpha_{pitch} \leq 14^\circ$, whilst for the membrane wing it extended over a greater range ($10^\circ \leq \alpha_{pitch} \leq 21^\circ$). Gresham *et al.*[6] noted that the change from large equilibrium angles to near-zero values coincided with the separation bubble becoming more symmetric across the wing span and eventually bursting as it reached the trailing-edge.

3. Self-excited roll oscillations about $\phi_{mean} \approx 0^\circ$

The third region was characterised by self-excited, limit-cycle roll oscillations about a near-zero mean angle. The onset of these oscillations occurred well below the stall angles of the wings; and the upper limit extended well above (see Figure 3). The mean amplitude of the quasi-sinusoidal

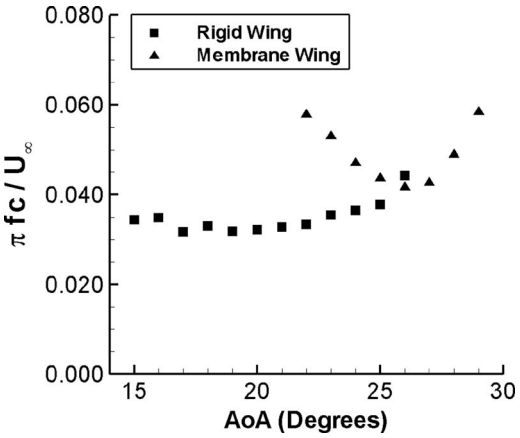

FIG. 5. Reduced frequency of the free-to-roll oscillations as a function of angle of attack for rigid and membrane wings. $Re_c = 46\,000$.

motions increased steadily with incidence up to a maximum value of $\phi = 50^\circ$ for the rigid wing and $\phi = 49^\circ$ for the membrane wing. Since the peak roll amplitude never passed $\pm 90^\circ$ there were no signs of autorotation, in contrast with earlier work.[6] This may be due to the differences in the leading-edge shape of the wings.

The key difference between the two wings tested here was the range of incidence angles for which significant rolling activity was observed: $15^\circ \leq \alpha_{\text{pitch}} \leq 27^\circ$ in the rigid case, but only $22^\circ \leq \alpha_{\text{pitch}} \leq 29^\circ$ for the membrane wing. This suggests that membrane wings can be less susceptible to wing rock than comparable rigid wings. The reasons are not obvious, however must be related to the variations of both the strength and location of the vortices.[2,6]

In addition to studying the magnitude of the roll oscillations, the spectral content of the signals was also analysed using an FFT method. The dominant frequency f_0 of the self-sustained roll oscillations are shown in Figure 5 in a dimensionless form. This figure shows that for both wings the largest amplitude of oscillations coincided with the lowest natural frequency. The membrane wing exhibited greater variation between the minimum and maximum frequencies across the range of self-excited wing rock (up to 40%); whereas for most of the rigid wing case the variation was less than 19%. The natural frequency of the roll oscillations depends on the governing parameters of this fluid-structure interaction, i.e., mass moment of inertia of the wing around the midspan axis and the roll-moment coefficient, which varies with angle of attack.[23]

4. Return to steady, near-zero roll angles

At high incidence angles the diminished influence of the tip vortices (both in terms of their strength and proximity to the wing surface), leads to a decrease in the wing rock amplitude. For $\alpha_{\text{pitch}} > 27^\circ$ for the rigid wing and $\alpha_{\text{pitch}} > 29^\circ$ for the membrane wing, the roll oscillations ceased and the wing returned to a steady, near-zero roll angle.

B. Dynamic pitching wings

Following on from the tests at stationary incidence angles, the study turned to simulation of gust conditions through periodic pitching of the wing. In the first instance, the mean pitch angle was chosen in the middle of the region of self-excited roll oscillations from the fixed-incidence cases. The pitching motion is defined as of $\alpha_{\text{pitch}} = \alpha_0 + A \sin(2\pi f_{\text{pitch}} t)$, where $\alpha_0 = 20^\circ$ for the rigid wing and $\alpha_0 = 26^\circ$ for the membrane wing. In order to reduce discrepancies in the test conditions for the rigid and membrane wings, the mean pitch angle A_0 was different for the two cases; reflecting the different angles at which self-excited roll oscillations occurred. Five values of pitch amplitude (A) were selected for investigation: $A = 1^\circ$, 2°, 3°, 4°, and 5°.

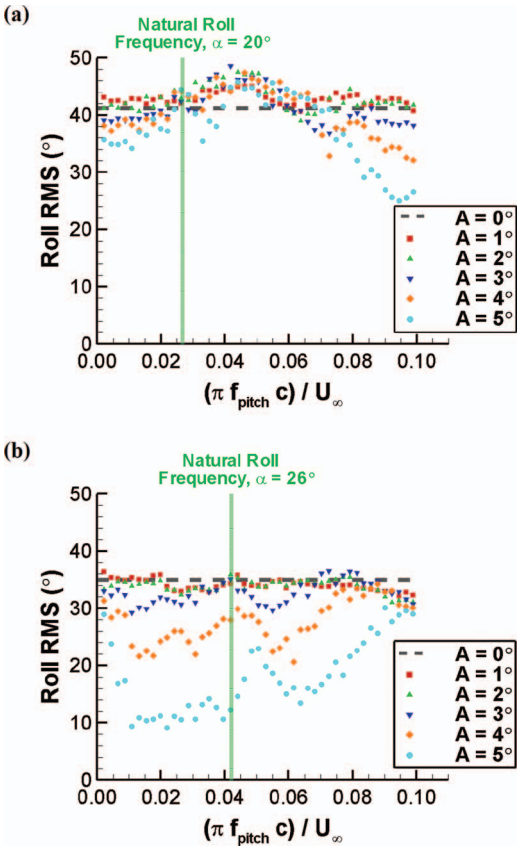

FIG. 6. RMS of roll angle as a function of pitch reduced frequency and pitch amplitude for (a) rigid wing with $\alpha_{\text{pitch}} = 20^\circ + A\cos(2\pi f_{\text{pitch}}\,t)$, (b) membrane wing with $\alpha_{\text{pitch}} = 26^\circ + A\cos(2\pi f_{\text{pitch}}\,t)$. $\text{Re}_c = 46\,000$.

Variation of the root-mean-square (RMS) of the roll angle is plotted as a function of pitch reduced frequency in Figures 6(a) and 6(b), and show significant differences between the rigid and membrane wings. For the rigid wing, the roll amplitude did not vary significantly between pitch amplitude cases and also did not diverge from the stationary wing value at the mean angle of attack (shown by the horizontal dashed line) by more than 18% until the pitch reduced frequency ($k_{\text{pitch}} = \pi f_{\text{pitch}} c/U_\infty$) exceeded 0.08 (Figure 6(a)). By contrast, the membrane wing exhibited a strong dependence on the pitch amplitude. In general, the rolling amplitude decreased with increasing pitch amplitude, resulting in a reduction in the roll RMS of up to 73% for $A = 5^\circ$ compared to the stationary wing baseline (Figure 6(b)) shown by the horizontal dashed line.

The variations in the roll amplitude with pitch frequency appeared to follow distinct peaks and troughs. In order to understand these further, the spectral content of the rolling signal was again analysed using an FFT algorithm. The three-dimensional plots in Figures 7 and 8 give the dimensionless dominant roll frequencies ($k_{\text{roll}} = \pi f_{\text{roll}}\, c/U_\infty$) and spectral amplitude of the wing rock signal as a function of the pitch reduced frequency ($k_{\text{pitch}} = \pi f_{\text{pitch}} c/U_\infty$) for the rigid and membrane wings. At low pitch amplitudes (Figures 7(a) and 8(a)), the roll frequency closely followed the natural roll frequency (f_0) for the stationary-incidence and the spectral amplitude did not vary significantly. However, as the pitch amplitude A was increased, the roll behaviour began to diverge from this quasi-state case: instead of following the line $f_{\text{roll}} = f_0$, the roll frequency became attracted first to the pitch frequency ($f_{\text{roll}} = f_{\text{pitch}}$) and then, at higher pitch frequencies, the subharmonics $f_{\text{roll}} = 1/2 f_{\text{pitch}}$ and $f_{\text{roll}} = 1/3 f_{\text{pitch}}$. These "lock-in" regions were centred on the points where the natural frequency line intersected the pitch frequency lines and can be most clearly seen in the rigid wing, $A = 3^\circ$ case (Figure 7(c)). The spectral amplitude of the dominant peaks was seen to reach a maximum at these intersection points. The results were indicative of the behaviour commonly

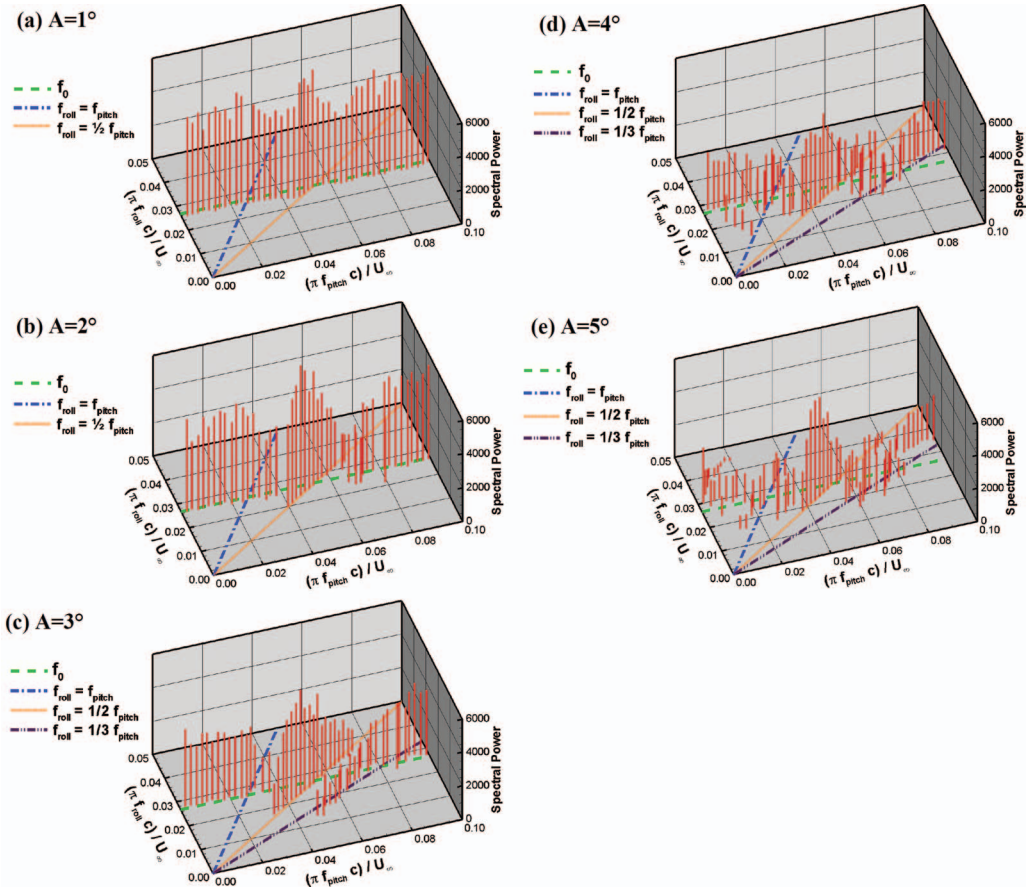

FIG. 7. Spectra of rolling motion as a function of reduced pitching frequency and pitch amplitude for rigid wing, $\alpha_{\text{pitch}} = 20^{\circ} + A\cos(2\pi f_{\text{pitch}}\, t)$. $\text{Re}_c = 46\,000$.

known as "synchronization", where the frequency and phase of weakly interacting signals become locked together.[10] Synchronization has been observed across a wide range of scientific disciplines including cardiorespiratory rhythms,[24] chirping crickets[25] and chaotic lasers.[26] It has also been reported previously in studies of fluid dynamics,[11–16] as discussed in the introduction to this paper.

Wakes and impinging shear flows generally exhibit the features of the self-sustained oscillators and synchronization when excited by external periodic forcing. Although we have a wake flow in our case, the "self-sustained oscillator" is not the wake flow, but the wing exhibiting roll oscillations. These self-excited roll oscillations result from the fluid-structure interaction. To give an idea, the natural roll frequencies of the wings are two orders of magnitude smaller than the vortex shedding frequency in the wake for the corresponding rigid low-aspect-ratio wing at zero roll angle.[20]

Reduced-order analytical models of wing rock at a fixed angle of attack are well known (for example, Elzebda *et al.*[23]). In these models, the equation of motion is solved as follows:

$$I_{xx}\ddot{\phi} = \frac{1}{2}\rho U_{\infty}^2 SbC_{ROLL}, \tag{2}$$

where ϕ is the roll angle, ρ is the density of sir, U_{∞} is the speed of the freestream, S is the planform area, b is the wing span, C_{ROLL} is the roll-moment coefficient, and I_{xx} is the mass moment of inertia of the wing around the midspan axis. Based on the test data, it is assumed that the roll-moment coefficient depends on the roll angle and its acceleration,

$$C_{ROLL} = a_1\phi + a_2\dot{\phi} + a_3\,|\phi|\,\dot{\phi} + a_4\,|\dot{\phi}|\,\dot{\phi}, \tag{3}$$

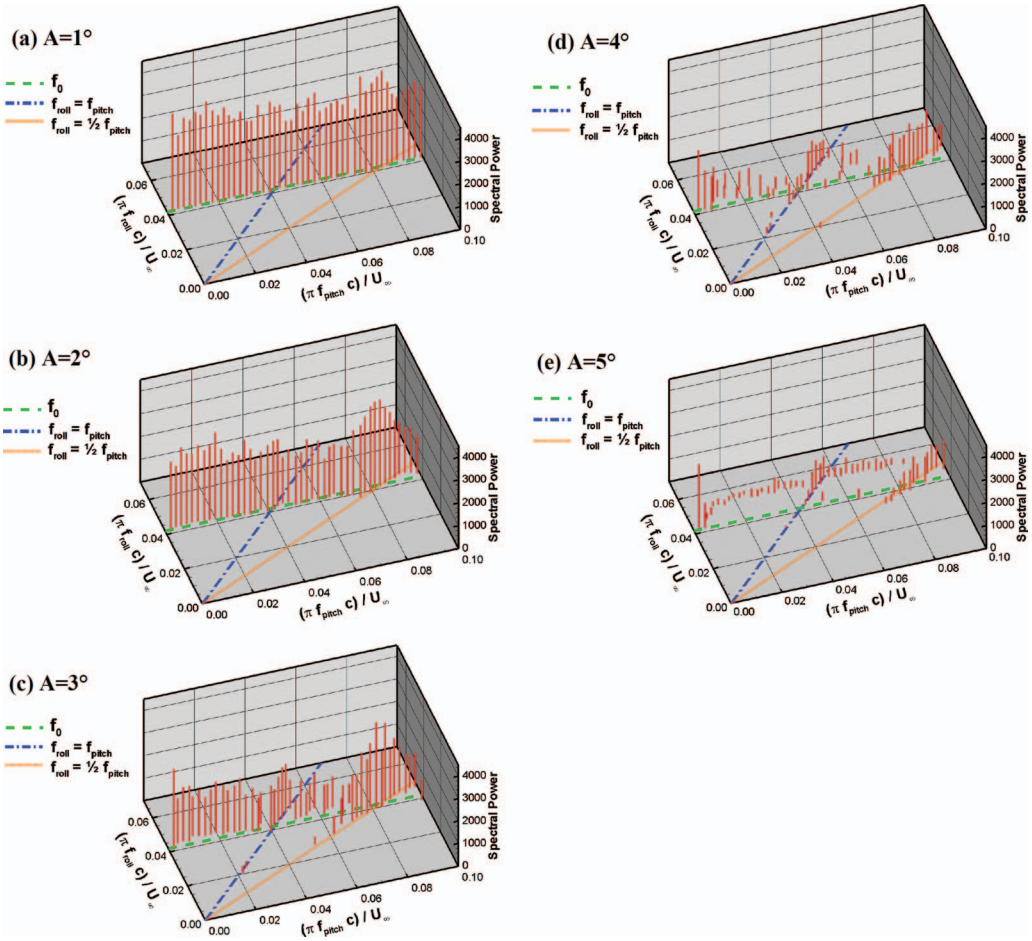

FIG. 8. Spectra of rolling motion as a function of reduced pitching frequency and pitch amplitude for membrane wing, $\alpha_{\text{pitch}} = 26^{\circ} + A\cos(2\pi f_{\text{pitch}}\, t)$. $\text{Re}_c = 46\,000$.

where the coefficients a_1, a_2, a_3, and a_4 depend on the angle of attack α. This nonlinear second-order differential equation was solved for fixed angles of attack by Elzebda *et al.*[23] In our case, the angle of attack varies periodically with time, resulting in a highly nonlinear system with external excitation.

For a slender delta wing, Khan *et al.*[17] seems to capture the synchronization for $f_{\text{pitch}} = 2f_0$, resulting in the roll oscillations with dominant frequency $f_{\text{roll}} \cong f_0$, although this was not commented on further. Hence, synchronization phenomenon may be generic for this type of fluid-structure interactions for widely different wing planforms.

Excitation may offer the potential to tune a self-sustained oscillator to an external frequency. For example friction-induced, self-excited oscillations of a mechanical system can be quenched by high-frequency external excitation.[27] For fluid flow, Pier[28] suggested that self-sustained oscillations may be controlled by a prescribed external frequency for better performance of the system. Hallberg and Strykowski[29] showed experimentally that a self-sustained oscillator (a low density jet) can be synchronized with an external periodic excitation, and the amplitude of the oscillations may be increased or decreased with respect to the no-forcing case (depending on the amplitude and frequency). From a control point of view, Figures 6–8 show this potential. For example, high-frequency excitation reduces the RMS of the roll oscillations for the rigid wing. There is even better reduction for the membrane wing, but not at high pitch frequencies.

Looking at the roll amplitude and spectra data together, it becomes clear that the peaks in the roll RMS (such as the one centred on $k_{\text{pitch}} \cong 0.045$ in Figure 6(a)) match the points where the $f_{\text{roll}} = 1/2f_{\text{pitch}}$ line crosses the natural frequency line (Figure 7(a)–7(e)). Similarly, the synchronization

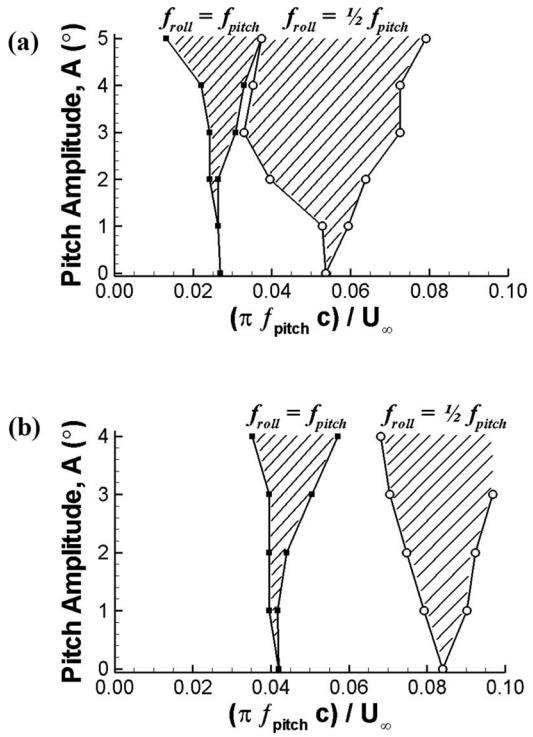

FIG. 9. "Arnold Tongue" plots showing boundary of roll frequency entrainment at different values of the pitch amplitude for (a) rigid wing, $\alpha_{pitch} = 20^\circ + A\cos(2\pi f_{pitch}\, t)$ and (b) membrane wing, $\alpha_{pitch} = 26^\circ + A\cos(2\pi f_{pitch}\, t)$. $Re_c = 46\,000$.

$f_{roll} = 1/2 f_{pitch}$ causes a local increase in the amplitude of the wing roll oscillations for the membrane wing. For this wing, the $A = 5^\circ$ case was also notable for a slightly different response of the roll angle. It was only at the very lowest pitching frequencies (where the system was operating in a quasi-steady manner) that the roll frequency ever matched the natural stationary wing frequency, f_0 (Figure 8(e)). At all other pitch frequencies there was an apparent shift to a higher natural frequency. Alteration of the natural self-excited frequency in the presence of an oscillating edge was previously observed for a jet-impinging flow.[15]

By plotting the boundaries of the frequency entrainments for the different pitch amplitudes it was possible to construct so-called "Arnold Tongue" diagrams (see Figure 9), named after the Russian mathematician Vladimir Arnold,[30] who applied the analysis to a biological phenomenon involving the beating frequency of the human heart. The broadening of the "tongues" as the pitch amplitude (and hence synchronous driving force) increases is a characteristic of these self-sustained oscillator systems.[26]

In the second set of periodic pitching experiments, the minimum pitch angles were selected in the oscillation-free region for the fixed-incidence cases, while the maximum pitch angles were in the region of the roll oscillations. Consequently, each cycle of the pitch motion took the wing in and out of the region where wing rock was observed in the stationary cases. A single pitch amplitude, $A = 5^\circ$, was chosen for the tests. The mean angle of attack α_0 was 15° for the rigid wing and 22° for the membrane wing.

Figure 10 shows the variation of the RMS roll angle as a function of pitch reduced frequency. Also shown are the corresponding values at the mean and maximum angles of attack for the fixed-incidence cases. There are regions of increased or decreased oscillations, which may be important from a control point of view. Figure 11 shows the spectra of the roll oscillations as a function of pitch reduced frequency. As with the first pitching tests, distinct peaks showed up in the RMS value of the roll angle (Figure 10), corresponding to the intersection of the fixed-incidence natural roll frequency f_0 with the pitch frequency and its subharmonics (Figure 11). Interestingly, whilst the rigid wing was entrained along both $f_{roll} = f_{pitch}$ and $f_{roll} = 1/2 f_{pitch}$ lines; the membrane wing showed only very

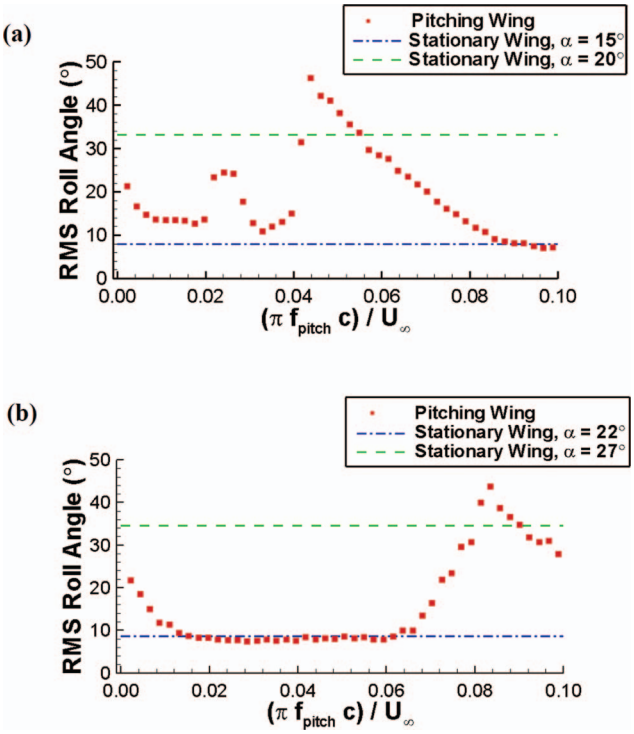

FIG. 10. Variation of RMS roll angle with pitch reduced frequency for (a) rigid wing, $\alpha_{\text{pitch}} = 15^\circ + 5^\circ\cos(2\pi f_{\text{pitch}}\,\text{t})$, and (b) membrane wing, $\alpha_{\text{pitch}} = 22^\circ + 5^\circ\cos(2\pi f_{\text{pitch}}\,\text{t})$. $\text{Re}_c = 46\,000$.

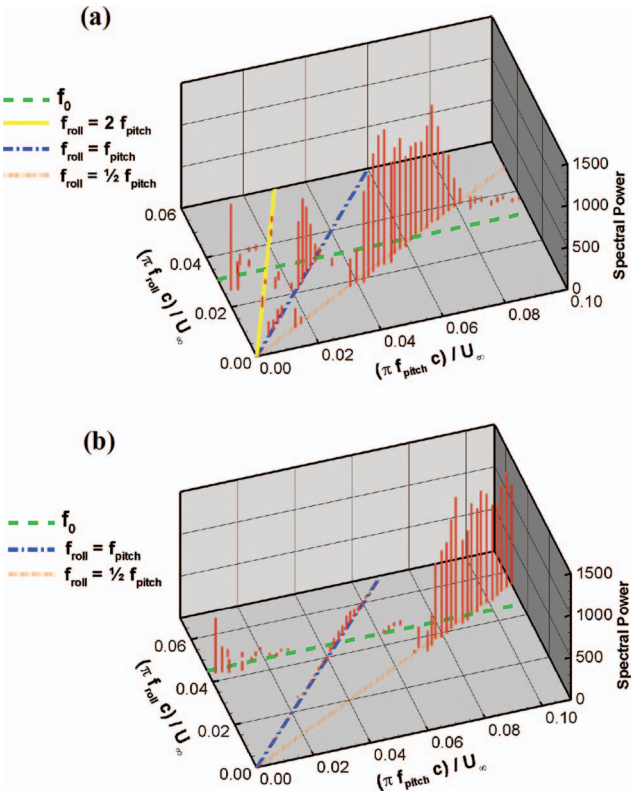

FIG. 11. Spectra of rolling motion as a function of reduced pitching frequency. Plot (a) corresponds to rigid wing with $\alpha_{\text{pitch}} = 15^\circ + 5^\circ\cos(2\pi f_{\text{pitch}}\text{t})$, whilst (b) corresponds to membrane wing with $\alpha_{\text{pitch}} = 22^\circ + 5^\circ\cos(2\pi f_{\text{pitch}}\text{t})$. $\text{Re}_c = 46\,000$.

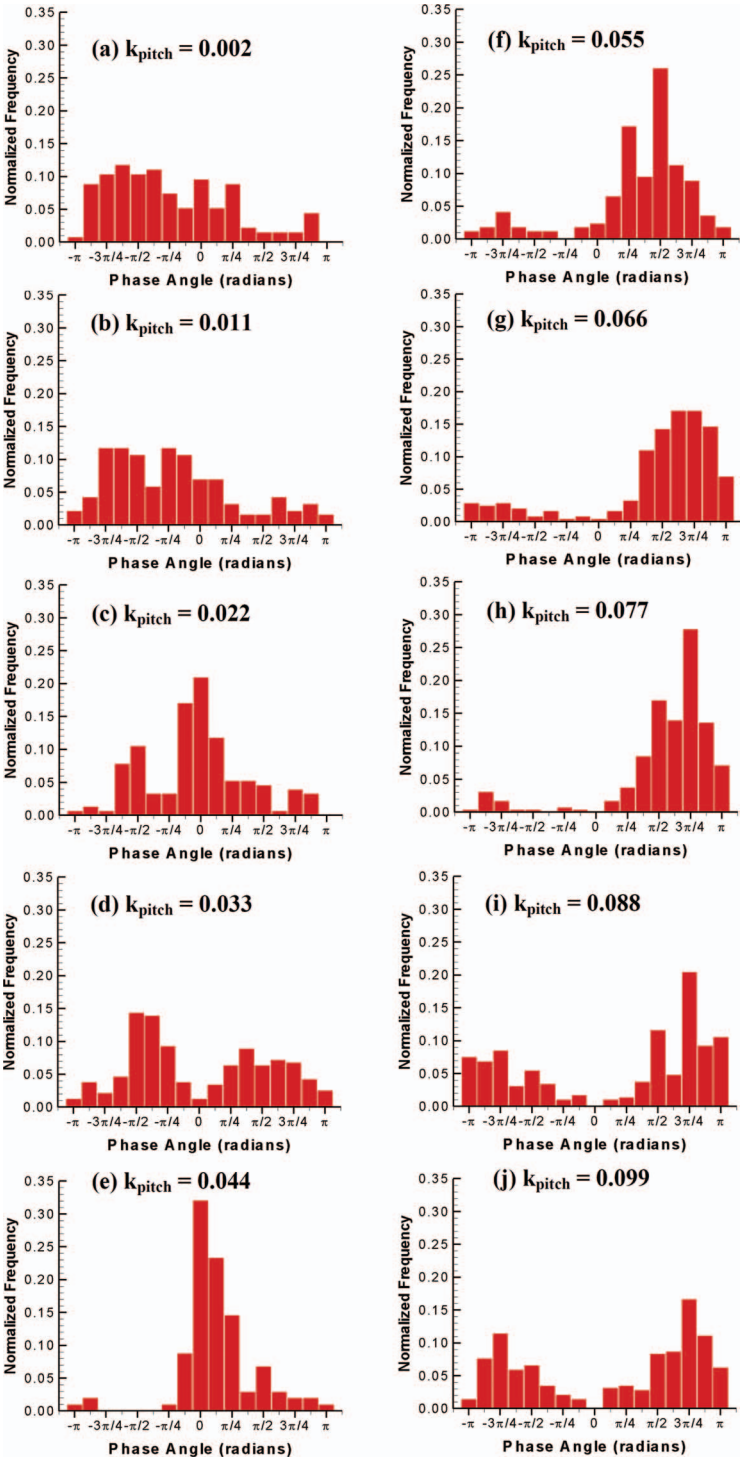

FIG. 12. Histograms showing how the phase angle between the pitch and roll motions changes as the pitch reduced frequency varies. Rigid wing, $\alpha_{pitch} = 15^\circ + 5^\circ\cos(2\pi f_{pitch}t)$. $Re_c = 46\,000$.

weak frequency entrainment at $f_{roll} = f_{pitch}$, but a very strong synchronization along $f_{roll} = 1/2f_{pitch}$. Comparing with previous tests (Figures 7 and 8), we reach the conclusion that the synchronization along $f_{roll} = 1/2f_{pitch}$ is always stronger for both wings.

In addition to the frequency analysis, with these tests we also explored the phase relationship between the pitch and roll signals. For a strong (or complete) synchronization, the phase angle is

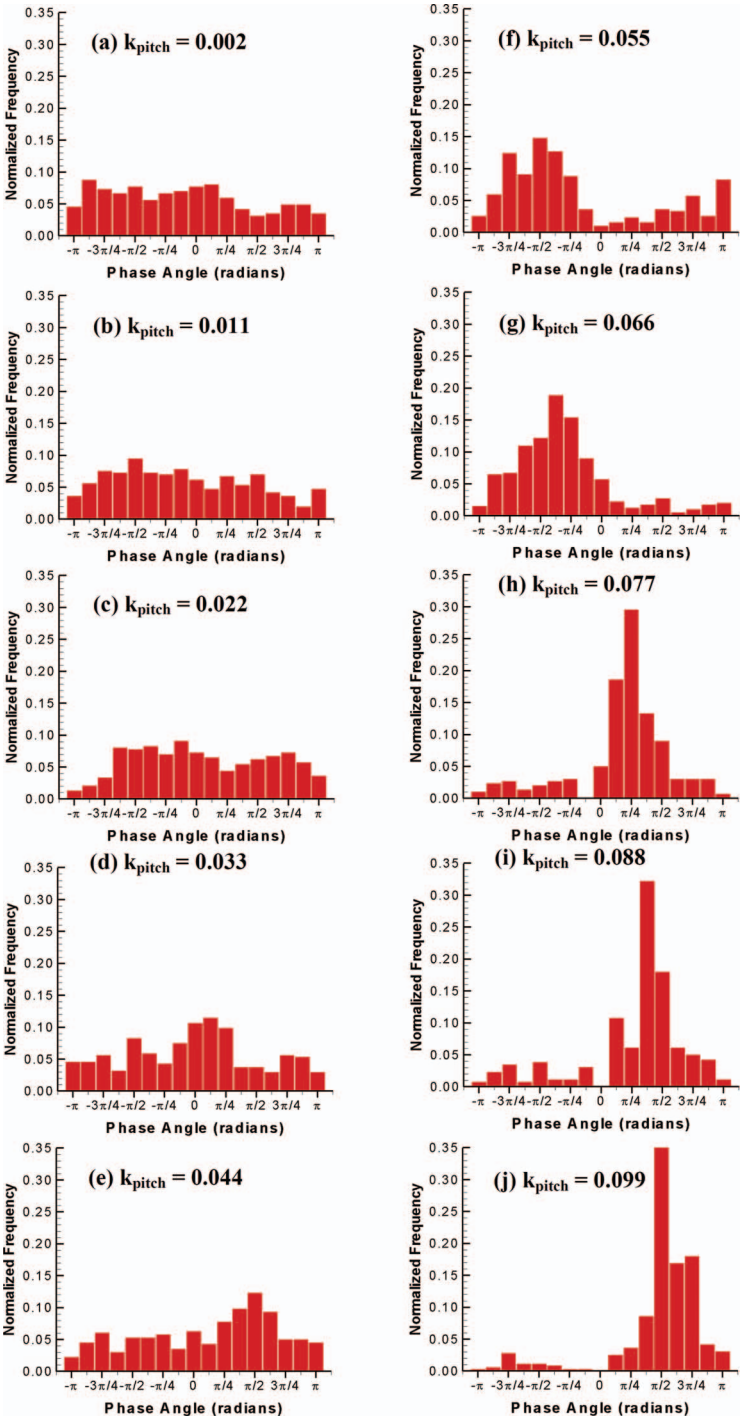

FIG. 13. Histograms showing how the phase angle between the pitch and roll motions changes as the pitch reduced frequency varies. Membrane wing, $\alpha_{pitch} = 22^{\circ} + 5^{\circ}\cos(2\pi f_{pitch}t)$. $Re_c = 46\,000$.

expected to lock and remain constant. However, for a weak synchronization, the phase does not stay constant, and may fluctuate in a random way.[31] The phase distribution is expected to be uniform in absence of synchronization and to have a well-defined peak in presence of synchronization. In Figures 12 and 13, phase angle histograms are plotted for various ascending values of the pitch reduced frequency for the rigid and membrane wings, respectively. A zero-crossing method was

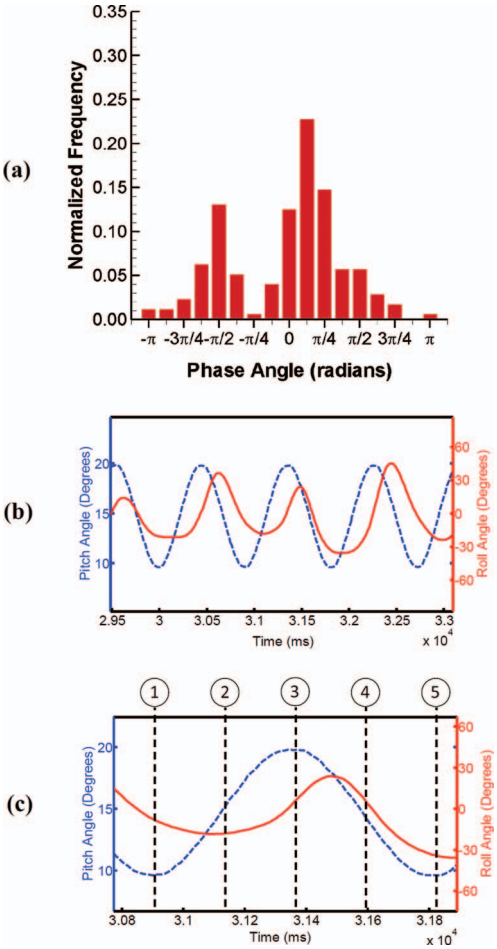

FIG. 14. Histogram showing the phase angle between the pitch and roll angles (a) and time history of the wing roll and pitch angles (b) and (c). Rigid wing, $\alpha_{pitch} = 15^\circ + 5^\circ\cos(2\pi f_{pitch}\, t)$, $k_{pitch} = 0.024$ and $Re_c = 46\,000$. Note that the numbered points in (c) correspond to the phase-locked PIV measurements in Figure 15.

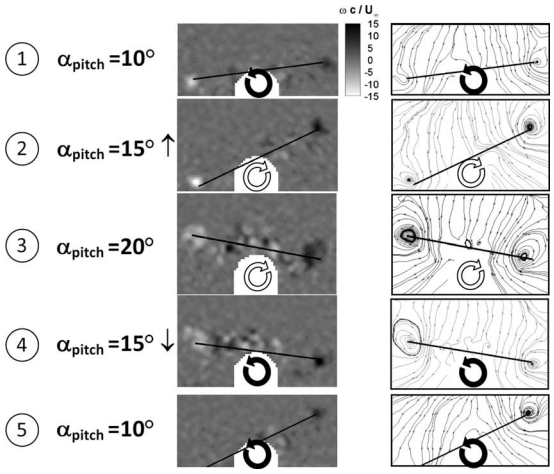

FIG. 15. Cross-stream PIV measurements phase-locked with rigid wing pitching motion as it goes through one complete pitching cycle. For this case ($\alpha_{pitch} = 15^\circ + 5^\circ\cos(2\pi f_{pitch} t)$, $k_{pitch} = 0.024$ and $Re_c = 46\,000$), the roll motion is entrained to the fundamental frequency of the pitching motion, i.e., one cycle of the pitch motion leads to one cycle of the roll motion. Contours of normalised vorticity are shown on the left and streamlines are plotted on the right. Numbers in circles correspond to the points in Figure 14(c). Arrows on the pitch labels beside each diagram indicate whether the wing is pitching up or down. Arrows on the plots indicate the direction of the roll rotation at that instance.

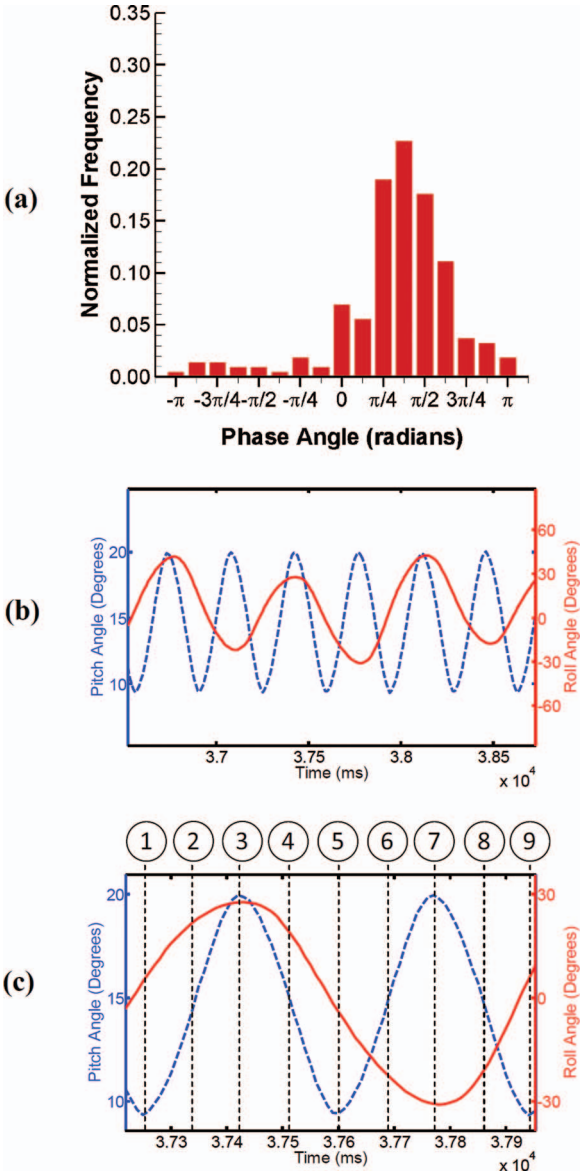

FIG. 16. Histogram showing the phase angle between the pitch and roll angles (a) and time history of the wing roll and pitch angles (b) and (c). Rigid wing, $\alpha_{pitch} = 15^\circ + 5^\circ\cos(2\pi f_{pitch}t)$, $k_{pitch} = 0.062$ and $Re_c = 46\,000$. Note that the numbered points in (c) correspond to the phase-locked PIV measurements in Figure 17.

used to identify the phase angle, with positive values indicating that the roll motion lagged the pitch. In cases where there was no locking of the pitch and roll frequencies, the phase angle is evenly distributed (Figure 13(a)). However, in the cases where the rolling frequency was locked-in to the pitch input or its subharmonics a strong peak appears in the histogram, signifying a statistical bias towards that particular phase angle (see Figure 12(e) or Figure 13(i)). The smearing of the phase histogram peaks in these experiments is indicative of a "noisy" system, where the phase-locking due to the forcing signal is disturbed by the presence of noise inputs.[31,32]

C. PIV flow-field analysis

Because the synchronization between pitch and roll motions only occurred in a statistical sense, it was not possible to take phase-averaged PIV measurements of the flow field. The results presented

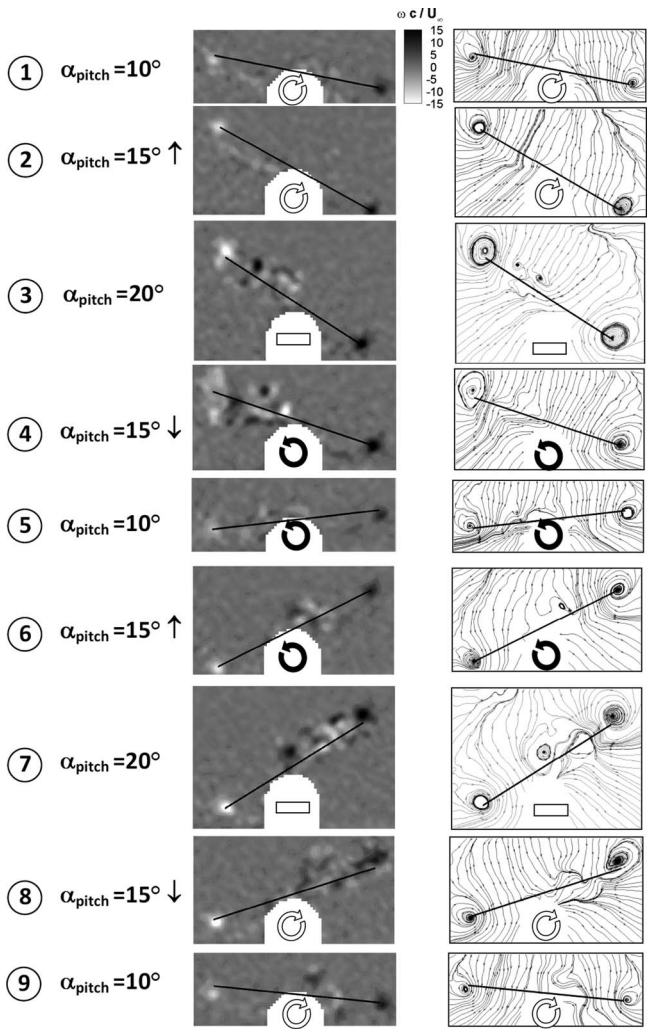

FIG. 17. Cross-stream PIV measurements phase-locked with rigid wing pitching motion as it goes through two complete pitching cycles. For this case ($\alpha_{pitch} = 15^\circ + 5^\circ\cos(2\pi f_{pitch}t)$, $k_{pitch} = 0.062$ and $Re_c = 46\,000$) the roll motion is entrained to the first subharmonic frequency of the pitching motion, i.e., two cycles of the pitch motion leads to one cycle of the roll motion. Contours of normalised vorticity are shown on the left and streamlines are plotted on the right. Numbers in circles correspond to the points in Figure 16(c). Arrows on the pitch labels beside each diagram indicate whether the wing is pitching up or down. Arrows on the plots indicate the direction of the roll rotation at that instance.

in this section are therefore instantaneous flow fields, selected so as to be representative of the average system behaviour. The PIV measurements were triggered by the pitching motion, with the capture rate set at four times the pitch frequency. Figures 14 and 15 refer to the rigid wing where the rolling motion is locked to the fundamental frequency of the pitch motion ($f_{roll} = f_{pitch}$). Figures 16 and 17 refer to the rigid wing locked to the pitch subharmonic ($f_{roll} = 1/2f_{pitch}$).

The histogram in Figure 14(a) indicates that the roll oscillations lagged the pitch motion by a phase angle of $1/8\pi$, which matches the data from the selected pitch and roll histories (Figures 14(b) and 14(c)). The five numbered points in Figure 14(c) correspond to the points of the pitching cycle at which PIV image pairs were taken. In Figure 15, vorticity contours (left) and streamlines (right) derived from these PIV images are presented. Immediately apparent are the large variations in vorticity between different points in the pitch cycle, and the presence of significant spanwise asymmetry. However, at all roll angles the tip vortices remain in the close proximity of the wing. It is evident that, near the largest roll angles, strengthening of the tip vortex provides the restoring rolling moment. This is consistent with previous findings.[6]

The difference in roll angle between the start and end of the pitch cycle (Figure 15) also highlights the influence that noise has in disrupting the phase-locking of the system. As discussed earlier, the absence of perfect phase locking is known to occur in "noisy" systems.

For the case of subharmonic synchronization shown in Figure 16, a roll phase lag of $3\pi/8$ is evident in Figure 16(a). The representative cycle shown in Figure 16(c) and the corresponding flow fields shown in Figure 17 indicate that the maximum and minimum roll angles occur near the maximum pitch angle. Even at the largest roll angles, the tip vortices remained close to the wing. Note that the flow is fully separated at the leading-edge for the rigid wing at these angles of attack. Strong asymmetries at small roll angles are indication of hysteresis effects that are known to exist in such flows.[5,6]

IV. CONCLUDING REMARKS

Experiments on free-to-roll rectangular wings with an aspect ratio of two have been conducted at a low Reynolds number. Both rigid and flexible (membrane) wings were investigated. The presence of self-excited wing-rock behaviour over a range of stationary incidence angles reinforced the idea that such oscillations are not confined to wings with swept leading edges. The onset of roll oscillations was confirmed to be well below the stall angle for both wings and the point at which they stopped was well above it. The angle of attack range for which rolling motions were observed was found to be 12° for the rigid wing but only 7° for the membrane wing, leading to the conclusion that under steady-incidence conditions membrane wings may be less susceptible to wing rock.

The fluid-structure interaction leading to a self-sustained oscillator was studied in forced periodic pitching motion. It was found that the frequency and phase properties of the roll oscillations became synchronized with those of the pitch waveform for certain values of the pitch amplitude and frequency. The foci of the synchronized regions were the points where the natural rolling frequency of the wing crossed lines representing the pitch frequency ($f_{roll} = f_{pitch}$) and two of its subharmonics ($f_{roll} = 1/2 f_{pitch}$ and $f_{roll} = 1/3 f_{pitch}$). In general, the synchronization along $f_{roll} = 1/2 f_{pitch}$ is stronger for both wings. The boundaries of each locked-in region extended either side of the focal pitch frequency, with the overall size of the region increasing with pitch amplitude. The regions of lock-in exhibited the well- known "Arnold tongue" shape. The influence of external noise to the system was observed through disturbances in the phase angle between the pitch and roll waveforms. Outside of the locked-in regions the phase angle showed no tendency towards any specific value; within the locked-in regions it tended towards a peak value. The effects of synchronization on wing rock behaviour were dependent on the wing, pitch frequency (f_{pitch}) and pitch amplitude (A). There are regions of increased or decreased roll oscillations, which may be important in minimizing the roll oscillations in gust encounters.

ACKNOWLEDGMENTS

This work was supported by the UK Engineering and Physical Sciences Research Council (EPSRC) studentship, and the Air Force Office of Scientific Research, Air Force Material Command, USAF under Grant Number FA8655-10-1-3093.

[1] A. S. Arena and R. C. Nelson, "Experimental investigations on limit-cycle wing rock of slender wings," J. Aircr. **31**(5), 1148–1155 (1994).
[2] J. Katz, "Wing/vortex interactions and wing rock," Prog. Aerosp. Sci. **35**(7), 727–750 (1999).
[3] N. T. Gresham, Z. Wang, and I. Gursul, "Vortex dynamics of free-to-roll slender and nonslender delta wings," J. Aircr. **47**(1), 292–302 (2010).
[4] N. T. Gresham, Z. Wang, and I. Gursul, "Effect of slenderness ratio on free-to-roll wing aerodynamics," J. Aircr. **48**(3), 1112–1116 (2011).
[5] N. T. Gresham, Z. J. Wang, and I. Gursul, "Self-induced roll oscillations of nonslender wings," AIAA J. **47**(3), 481–483 (2009).
[6] N. T. Gresham, Z. J. Wang, and I. Gursul, "Low Reynolds number aerodynamics of free-to-roll low aspect ratio wings," Exp. Fluids **49**(1), 11–25 (2010).
[7] T. J. Mueller and J. D. DeLaurier, "Aerodynamics of small vehicles," Annu. Rev. Fluid Mech. **35**, 89–111 (2003).

[8] W. Shyy, M. Berg, and D. Ljungqvist, "Flapping and flexible wings for biological and micro air vehicles," Prog. Aerosp. Sci. **35**(5), 455–505 (1999).
[9] I. Gursul, "Vortex flows on UAVs: Issues and challenges," Aeronaut. J. **108**(1090), 597–610 (2004).
[10] A. Pikovsky, M. Rosenblum, and J. Kurths, *Synchronization: A Universal Concept in Nonlinear Sciences* (Cambridge University Press, 2003), Chap. 3.
[11] P. K. Stansby, "Locking-on of vortex shedding due to cross-stream vibration of circular cylinders in uniform and shear flows," J. Fluid Mech. **74**, 641–665 (1976).
[12] E. de Langre, "Frequency lock-in is caused by coupled-mode flutter," J. Fluids Struct. **22**(6-7), 783–791 (2006).
[13] G. E. Karniadakis and G. S. Triantafyllou, "Frequency selection and asymptotic states in laminar wakes," J. Fluid Mech. **199**, 441–469 (1989).
[14] J. Young and J. C. S. Lai, "Vortex lock-in phenomenon in the wake of a plunging airfoil," AIAA J. **45**(2), 485–490 (2007).
[15] T. Staubli and D. Rockwell, "Interaction of an unstable planar jet with an oscillating leading-edge," J. Fluid Mech. **176**, 135–167 (1987).
[16] D. E. Raveh and E. H. Dowell, "Frequency lock-in phenomenon for oscillating airfoils in buffeting flows," J. Fluids Struct. **27**(1), 89–104 (2011).
[17] M. J. Khan, A. Ahmed, and D. C. Oehl, "Response of free-to-roll slender delta wings to pitching and plunging," J. Aircr. **43**(1), 275–278 (2006).
[18] R. Smith and W. Shyy, "Computation of aerodynamic coefficients for a flexible membrane airfoil in turbulent flow: A comparison with classical theory," Phys. Fluids **8**(12), 3346–3353 (1996).
[19] R. Albertani, B. Stanford, J. P. Hubner, and P. G. Ifju, "Aerodynamic coefficients and deformation measurements on flexible micro air vehicle wings," Exp. Mech. **47**(5), 625–635 (2007).
[20] P. Rojratsirikul, M. S. Genc, Z. Wang, and I. Gursul, "Flow-induced vibrations of low aspect ratio rectangular membrane wings," J. Fluids Struct. **27**, 1296–1309 (2011).
[21] A. Song, X. Tian, E. Israeli, R. Galvao, K. Bishop, S. Swartz, and K. Breuer, "Aeromechanics of Membrane Wings with Implications for Animal Flight," AIAA J. **46**(8), 2096–2106 (2008).
[22] Y. S. Lian, W. Shyy, D. Viieru, and B. N. Zhang, "Membrane wing aerodynamics for micro air vehicles," Prog. Aerosp. Sci. **39**(6-7), 425–465 (2003).
[23] J. M. Elzebda, A. H. Nayfeh, and D. T. Mook, "Development of an analytical model of wing rock for slender delta wings," J. Aircr. **26**, 737–743 (1989).
[24] C. Schafer, M. G. Rosenblum, H. H. Abel, and J. Kurths, "Synchronization in the human cardiorespiratory system," Phys. Rev. E **60**, 857–870 (1999).
[25] L. Wang, H. Shi, and Y. X. Sun, "Induced synchronization of a mobile agent network by phase locking," Phys. Rev. E **82**(4), 046222(1)–046222(6) (2010).
[26] M. Rosenblum and A. Pikovsky, "Synchronization: from pendulum clocks to chaotic lasers and chemical oscillators," Contemp. Phys. **44**(5), 401–416 (2003).
[27] J. J. Thomson, "Using fast vibrations to quench friction-induced oscillations," J. Sound Vib. **228**, 1079–1102 (1999).
[28] B. Pier, "Open-loop control of absolutely unstable domains," Proc. R. Soc. London A **459**, 1105–1115 (2003).
[29] M. P. Hallberg and P. J. Strykowski, "Open-loop control of fully nonlinear self-excited oscillations," Phys. Fluids **20**, 041703 (2008).
[30] V. I. Arnold, "Cardiac arrhythmias and circle mappings," Chaos **1**(1), 20–24 (1991).
[31] M. G. Rosenblum, J. Kurths, A. Pikovsky, C. Schafer, P. Tass, and H. H. Abel, "Synchronization in noisy systems and cardiorespiratory interaction," IEEE Eng. Med. Biol. Mag. **17**(6), 46–53 (1998).
[32] A. B. Neiman, D. F. Russell, X. Pei, W. Wojtenek, J. Twitty, E. Simonotto, B. A. Wettring, E. Wagner, L. A. Wilkens, and F. Moss, "Stochastic synchronization of electroreceptors in paddlefish," Int. J. Bifurcation Chaos Appl. Sci. Eng. **10**(11), 2499–2517 (2000).